APPENDIX A: THE METAL LINE SPECTRUM IN BD+10°2179

Table A1. Line by line abundances of the non-LTE analysis of BD+10°2179. Abundances ϵ with respect to $\log \mu_X \epsilon_X = 12.15$, where μ_X is the atomic weight of element X.

Line	λ (Å)	χ(eV)	$\log gf$	Accu.	Source	Abun.
Hα	6562.819	10.20	0.71000	AAA	WF	8.37
Hβ	4861.333	10.20	−0.01996	AAA	WF	8.36
Hγ	4340.471	10.20	−0.44666	AAA	WF	8.36
Hδ	4101.742	10.20	−0.75243	AAA	WF	8.36
C I	4762.313	7.48	−2.463	C	WFD	9.77
C I	4762.533	7.48	−2.335	C	WFD	
C I	4771.742	7.49	−1.866	C	WFD	9.70
C I	4775.898	7.49	−2.304	C	WFD	9.84
C I	4932.049	7.68	−1.703	B	LP	9.57
C I	5052.167	7.68	−1.447	C	LP	9.67
C I	5380.337	7.68	−1.615	B	WFD	9.65
C I	6013.213	8.65	−1.673	D	WFD	9.56
C I	6587.610	8.54	−1.003	B	WFD	9.58
C I	7115.172	8.64	−0.935	B−	WFD	9.72
C I	7115.182	8.64	−1.473	B	WFD	
C II	4267.001	18.05	0.562	C+	WFD	9.78
C II	4267.261	18.05	0.717	C+	WFD	
C II	4267.261	18.05	−0.584	C+	WFD	
C II	4737.966	13.72	−3.444	B+	WFD	9.57
C II	4744.766	13.72	−3.111	B+	WFD	9.52
C II	4747.279	13.72	−3.820	B+	WFD	9.55
C II	5137.257	20.70	−0.911	B	WFD	9.76
C II	5139.174	20.70	−0.707	B	WFD	9.82
C II	5143.495	20.70	−0.212	B	WFD	9.89
C II	5145.165	20.71	0.189	B	WFD	9.93
C II	5535.353	19.49	−1.493	B	WFD	9.93
C II	5537.609	19.49	−1.794	B	WFD	9.90
C II	6578.052	14.45	−0.087	C+	N02	9.65
C II	6582.882	14.45	−0.388	C+	N02	
C II	6727.070	22.53	−1.065	B	WFD	9.74
C II	6727.260	22.53	−0.919	B	WFD	
C II	6731.070	22.53	−0.862	B	WFD	9.77
C II	6733.581	22.53	−1.066	B	WFD	9.75
C II	6734.003	22.53	−1.009	B	WFD	
C II	6738.606	22.53	−0.529	B	WFD	9.82
C II	6742.428	22.53	−0.920	B	WFD	9.78
C II	6750.536	22.54	−0.229	B	WFD	9.79
C II	6755.161	22.54	−1.010	B	WFD	9.75
C II	6779.942	20.70	0.025	B	WFD	9.96
C II	6783.908	20.71	0.304	B	WFD	9.86
C II	6787.207	20.70	−0.377	B	WFD	9.93
C II	6791.466	20.70	−0.270	B	WFD	9.92
C II	6798.104	20.70	−1.077	B	WFD	9.82
C II	6800.683	20.71	−0.343	B	WFD	9.80
C II	6812.280	20.71	−1.300	B	WFD	9.54
C III	4186.900	40.01	0.918	B	WFD	9.76
C III	4647.418	29.53	0.070	B+	WFD	9.67
C III	4650.246	29.53	−0.151	B+	WFD	9.73
N I	7442.298	10.33	−0.384	B+	WFD	7.99
N I	7468.312	10.34	−0.189	B+	WFD	7.86
N I	8680.282	10.34	0.346	B+	WFD	7.88
N I	8683.403	10.33	0.086	B+	WFD	7.93
N I	8686.149	10.33	−0.305	B+	WFD	8.01
N I	8703.247	10.33	−0.310	B+	WFD	7.93

Table A1 continued.

Line	λ (Å)	χ(eV)	log gf	Accu.	Source	Abun.
N II	3955.851	21.15	−0.813	B	WFD	7.99
N II	3994.997	18.50	0.163	B	FFT	8.03
N II	4035.081	23.12	0.599	B	BB89	7.89
N II	4041.310	23.14	0.748	B	MAR	7.97
N II	4043.532	23.13	0.440	C	MAR	8.19
N II	4176.159	23.20	0.316	B	MAR	8.04
N II	4227.736	21.60	−0.060	B	WFD	8.03
N II	4236.927	23.24	0.383	X	KB	7.84
N II	4241.755	23.24	0.210	X	KB	7.88
N II	4447.030	20.41	0.221	B	FFT	7.92
N II	4507.560	20.67	−0.817	B	WFD	7.92
N II	4530.410	23.47	0.604	C+	MAR	7.99
N II	4601.478	18.47	−0.452	B+	FFT	8.10
N II	4607.153	18.46	−0.522	B+	FFT	8.09
N II	4613.868	18.47	−0.692	B+	FFT	7.99
N II	4630.539	18.48	0.080	B+	FFT	8.22
N II	4643.086	18.48	−0.371	B+	FFT	8.06
N II	4654.531	18.50	−1.404	C+	WFD	7.84
N II	4667.208	18.50	−1.533	C+	WFD	7.94
N II	4694.642	23.57	0.100	X	KB	8.21
N II	4788.138	20.65	−0.366	B	FFT	7.99
N II	4793.648	20.65	−1.032	B+	FFT	8.04
N II	4987.376	20.94	−0.584	B	FFT	8.03
N II	5001.474	20.65	0.435	B	FFT	8.10
N II	5002.703	18.46	−1.022	B+	WFD	7.99
N II	5005.150	20.67	0.587	B	FFT	8.24
N II	5007.328	20.94	0.145	B	FFT	8.15
N II	5010.621	18.47	−0.607	B+	WFD	8.07
N II	5025.659	20.67	−0.557	B	FFT	8.11
N II	5452.070	21.15	−0.783	B	FFT	8.13
N II	5462.581	21.15	−0.826	B+	FFT	7.78
N II	5480.050	21.16	−0.711	B+	FFT	8.08
N II	5495.655	21.16	−0.220	B+	FFT	8.01
N II	5666.629	18.47	−0.104	B+	MAR	8.14
N II	5676.017	18.46	−0.356	B+	MAR	8.10
N II	5679.558	18.48	0.221	B+	MAR	8.18
N II	5686.213	18.47	−0.586	B+	FFT	8.14
N II	5710.766	18.48	−0.466	B	MAR	8.01
N II	5747.300	18.50	−1.092	B+	FFT	8.09
N II	5767.446	18.50	−1.447	B	FFT	7.98
N II	5931.782	21.15	0.047	A	FFT	7.99
N II	5941.654	21.16	0.307	A	FFT	8.18
N II	6379.627	18.47	−1.188	C+	FFT	8.05
N II	6482.048	18.50	−0.311	B+	FFT	8.18
N II	6610.562	21.60	0.440	B	FFT	8.15
O I	7771.944	9.15	0.354	A	FFT	7.40
O I	7774.166	9.15	0.207	A	FFT	
O I	7775.388	9.15	−0.015	A	FFT	
O II	3911.957	25.66	−0.014	B+	FFT	7.59
O II	3912.107	25.66	−0.907	B+	FFT	
O II	4345.560	22.98	−0.342	B+	FFT	7.48
O II	4349.426	23.00	0.073	B+	FFT	7.50
O II	4366.892	23.00	−0.333	B+	FFT	7.47
O II	4414.905	23.44	0.207	B	FFT	7.54
O II	4596.175	25.66	0.180	B+	FFT	7.45
O II	4641.810	22.98	0.066	B+	FFT	7.50
O II	4650.839	22.97	−0.349	B+	FFT	7.58
O II	4676.235	23.00	−0.410	B+	FFT	7.53
O II	4705.352	26.25	0.533	B+	FFT	7.53

Table A1 continued.

Line	λ (Å)	χ(eV)	log gf	Accu.	Source	Abun.
Ne I	5764.419	18.56	−0.316	B	B08	8.14
Ne I	5852.488	16.85	−0.454	B	B08	8.07
Ne I	5881.895	16.62	−0.792	B	B08	7.91
Ne I	5944.834	16.62	−0.636	B	B08	8.05
Ne I	6029.997	16.67	−1.026	B	FFT	7.98
Ne I	6074.338	16.67	−0.473	B+	FFT	7.92
Ne I	6143.063	16.62	−0.070	B+	FFT	7.90
Ne I	6163.594	16.72	−0.598	B+	FFT	8.04
Ne I	6217.281	16.62	−0.943	B	FFT	7.88
Ne I	6266.495	16.72	−0.331	B+	FFT	8.00
Ne I	6334.428	16.62	−0.277	B+	FFT	7.92
Ne I	6506.528	16.67	−0.002	B+	FFT	7.90
Ne I	6532.882	16.72	−0.670	B+	FFT	8.10
Ne I	6598.953	16.85	−0.360	B	B08	8.18
Ne I	6717.043	16.84	−0.346	B+	FFT	8.01
Ne I	7032.413	16.62	−0.222	B+	FFT	7.90
Mg II	4481.126	8.86	0.730	B	FW	6.89
Mg II	4481.150	8.86	−0.570	B	FW	
Mg II	4481.325	8.86	0.575	B	FW	
Mg II	4851.082	11.63	−0.424	C	CA	6.92
Mg II	6545.973	11.63	0.408	C	CA	7.06
Mg II	7877.054	10.00	0.391	A+	FFTI	6.92
Mg II	7896.042	10.00	−0.308	A	FFTI	7.01
Mg II	7896.366	10.00	0.647	A+	FFTI	
Al II	4663.046	10.60	−0.241	A+	FFTI	5.84
Al II	6243.073	13.08	−1.250	X	KB	5.79
Al II	6243.203	13.08	−0.080	X	KB	
Al II	6243.367	13.08	0.670	X	KB	
Al II	7042.083	11.32	0.332	A+	FFTI	5.86
Al III	4149.913	20.55	0.626	A+	FFTI	5.88
Al III	4149.968	20.55	−0.674	A+	FFTI	
Al III	4479.885	20.78	0.900	X	KB	5.78
Al III	4479.971	20.78	1.020	X	KB	
Al III	4480.009	20.78	−0.530	X	KB	
Al III	4512.565	17.81	0.408	A+	FFTI	5.78
Al III	4528.945	17.82	−0.291	A+	FFTI	5.80
Al III	4529.189	17.82	0.663	A+	FFTI	
Al III	5696.604	15.64	0.232	A+	FFTI	5.89
Al III	5722.730	15.64	−0.071	A+	FFTI	5.88
Si II	4128.054	9.84	0.31	C	WSM	7.12
Si II	4130.872	9.84	−0.84	E	WSM	7.03
Si II	4130.894	9.84	0.462	C	WSM	
Si II	5055.984	10.07	0.42	D+	WSM	7.07
Si II	5056.317	10.07	−0.53	E	WSM	
Si II	6371.371	8.12	−0.126	C+	FFTI	7.24
Si III	4338.500	19.02	−1.673	C+	FFTI	7.08
Si III	4567.840	19.02	0.068	B+	FFTI	7.12
Si III	4574.757	19.02	−0.409	B	FFTI	7.24
Si III	4813.333	25.98	0.653	B	CT	7.12
Si III	4828.951	25.99	0.870	B	CT	7.18
Si III	4829.030	25.99	−0.661	B	CT	
Si III	4829.111	25.99	−0.682	B	CT	
Si III	4829.214	25.99	−2.201	C	CT	
Si III	5739.734	19.72	−0.078	B	FFTI	7.13

Table A1 continued.

Line	λ (Å)	χ(eV)	log gf	Accu.	Source	Abun.
S II	4153.068	15.90	0.62	D	WSM	6.84
S II	4162.665	15.94	0.78	D	WSM	6.76
S II	4189.681	15.90	−0.05	E	WSM	6.90
S II	4282.595	16.10	−0.01	E	WSM	6.76
S II	4815.552	13.67	0.09	D	WSM	6.80
S II	5428.655	13.58	−0.13	D	WSM	6.83
S II	5432.797	13.62	0.26	D	WSM	6.86
S II	5473.614	13.58	−0.18	D	WSM	6.89
S II	5509.705	13.62	−0.14	D	WSM	6.89
Ar II	4426.001	16.75	0.195	B+	FFTI	5.89
Ar II	4430.189	16.81	−0.158	B	FFTI	5.90
Ar II	4657.900	17.14	−0.245	B	FFTI	5.86
Ar II	4764.864	17.27	−0.269	B	FFTI	6.06
Ar II	4806.020	16.64	0.235	B+	FFTI	5.90
Ar II	4847.810	16.75	−0.214	B	FFTI	5.86
Ar II	4879.863	17.14	0.544	B+	FFTI	6.00
Fe II	4296.566	2.70	−3.01	D	FMW	6.67
Fe II	5018.440	2.89	−1.22	C	FMW	6.51
Fe II	5169.033	2.89	−0.87	C	FMW	6.40
Fe III	4164.731	20.63	0.92	X	KB	6.67
Fe III	4164.916	24.65	1.01	X	KB	
Fe III	4395.755	8.26	−2.60	X	KB	6.43
Fe III	4431.019	8.25	−2.572	X	KB	6.57
Fe III	5156.111	8.64	−2.02	X	KB	6.62

accuracy indicators – uncertainties within: AAA: 0.3%; AA: 1%; A: 3%; B: 10%; C: 25%; D: 50%; E: >50%; X: unknown
sources of gf-values – B08: K. Butler, from Breit-Pauli R-matrix calculations as outlined in Morel & Butler (2008); BB89: Becker & Butler (1989); CA: Coulomb approximation, Bates & Damgaard (1949); CT: Callegari & Trigueiros (1998) FFT: Froese Fischer & Tachiev (2004); FFTI: Froese Fischer et al. (2006); FW Fuhr & Wiese (1998); FMW: Fuhr et al. (1988); KB: Kurucz & Bell (1995); LP: Luo & Pradhan (1989); MAR: Mar et al. (2000); N02: Nahar (2002); WF: Wiese & Fuhr (2009); WFD: Wiese et al. (1996); WSM: Wiese et al. (1969).
sources of Stark broadening parameters – H I: Vidal et al. (1973); C I: Griem (1974), Cowley (1971); Si II: Lanz et al. (1988), Griem (1974), Cowley (1971); C II, N I/II, Mg II: Griem (1964, 1974), Cowley (1971); C III, O I/II, Ne I, Al II/III, Si III, S II, Ar II, Fe II/III: Cowley (1971).

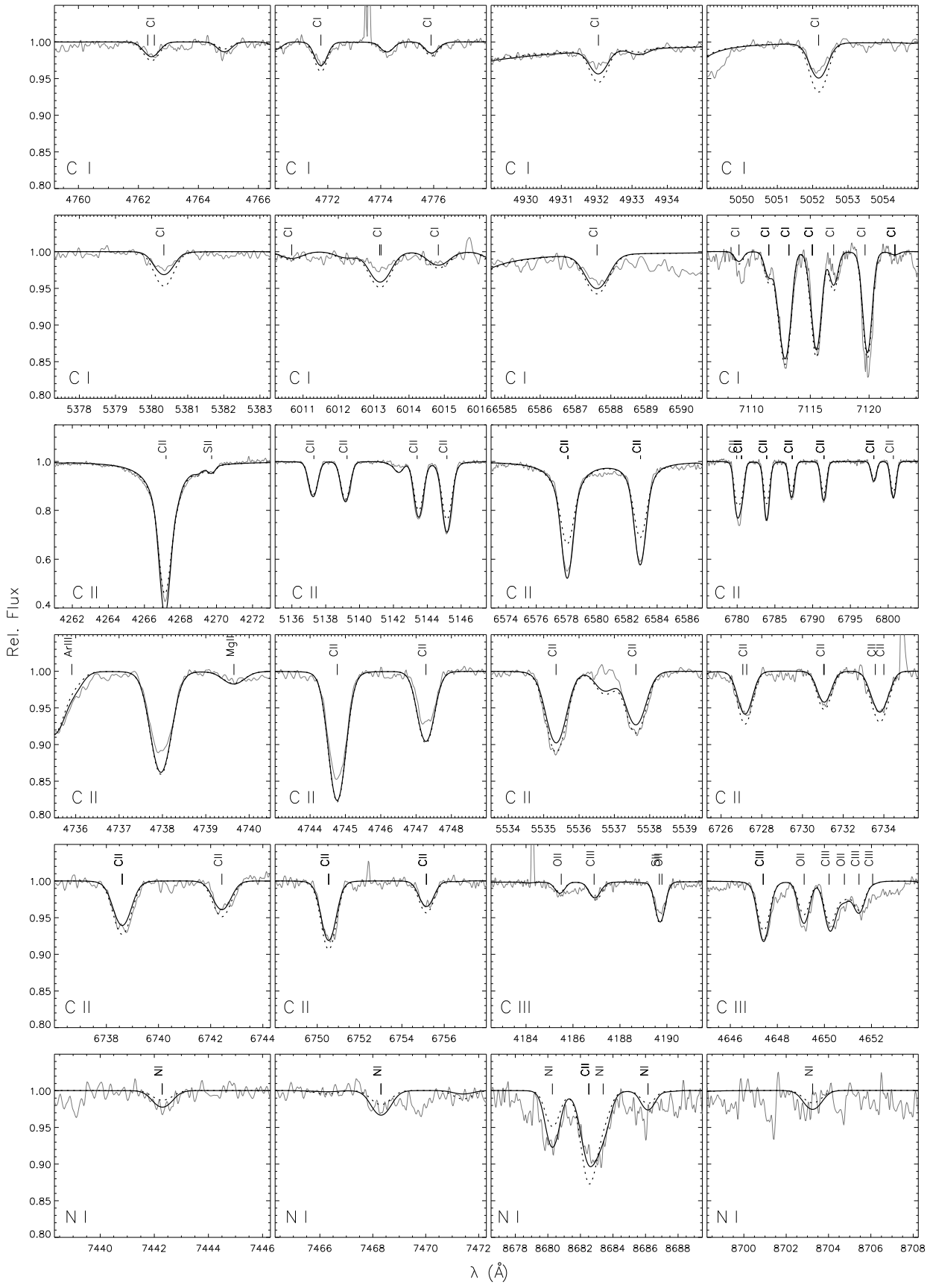

Figure A1. Like Fig. **??**, for analysed C I/II/III and N I lines.

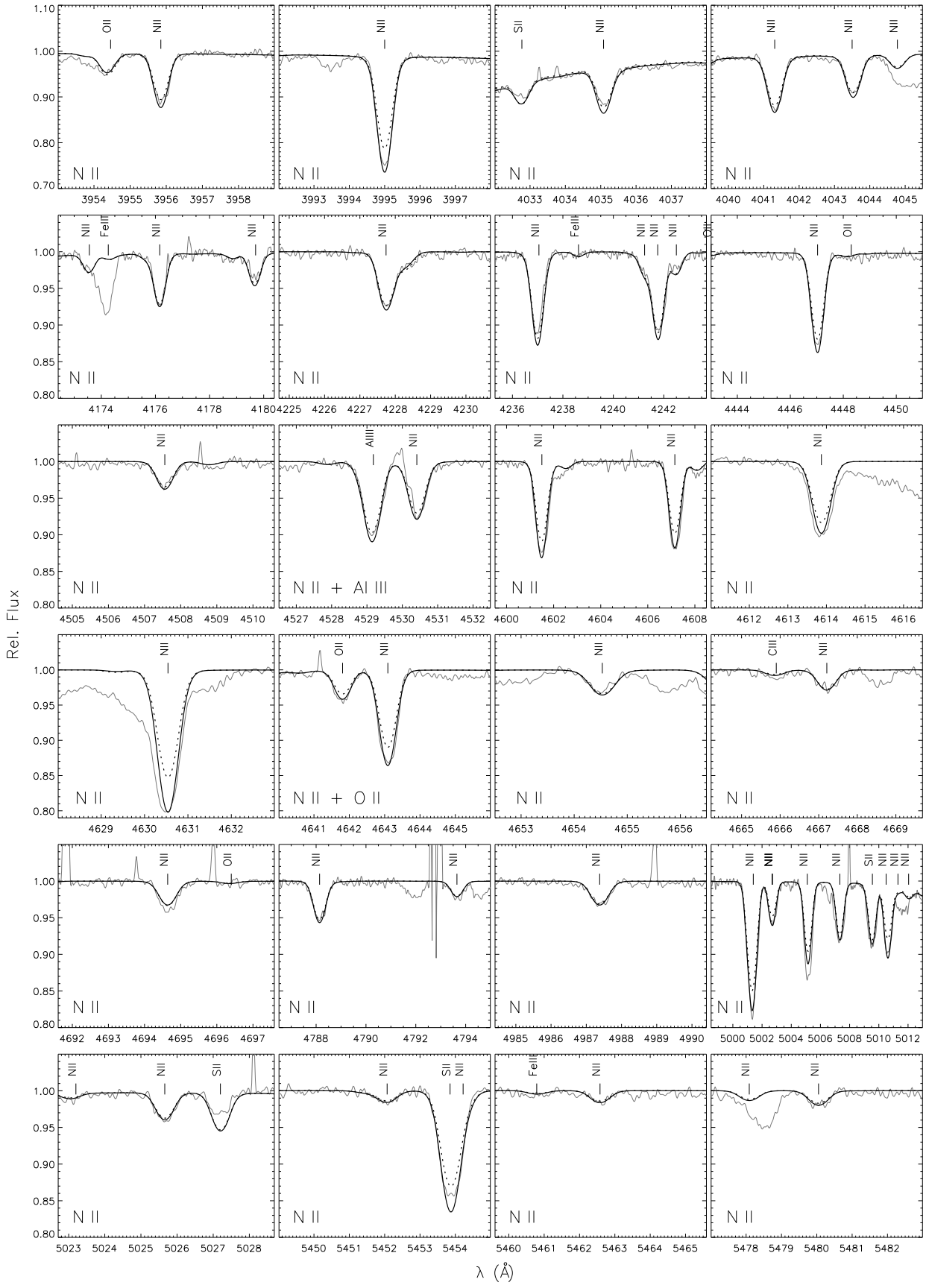

Figure A2. Like Fig. **??**, for analysed N II lines.

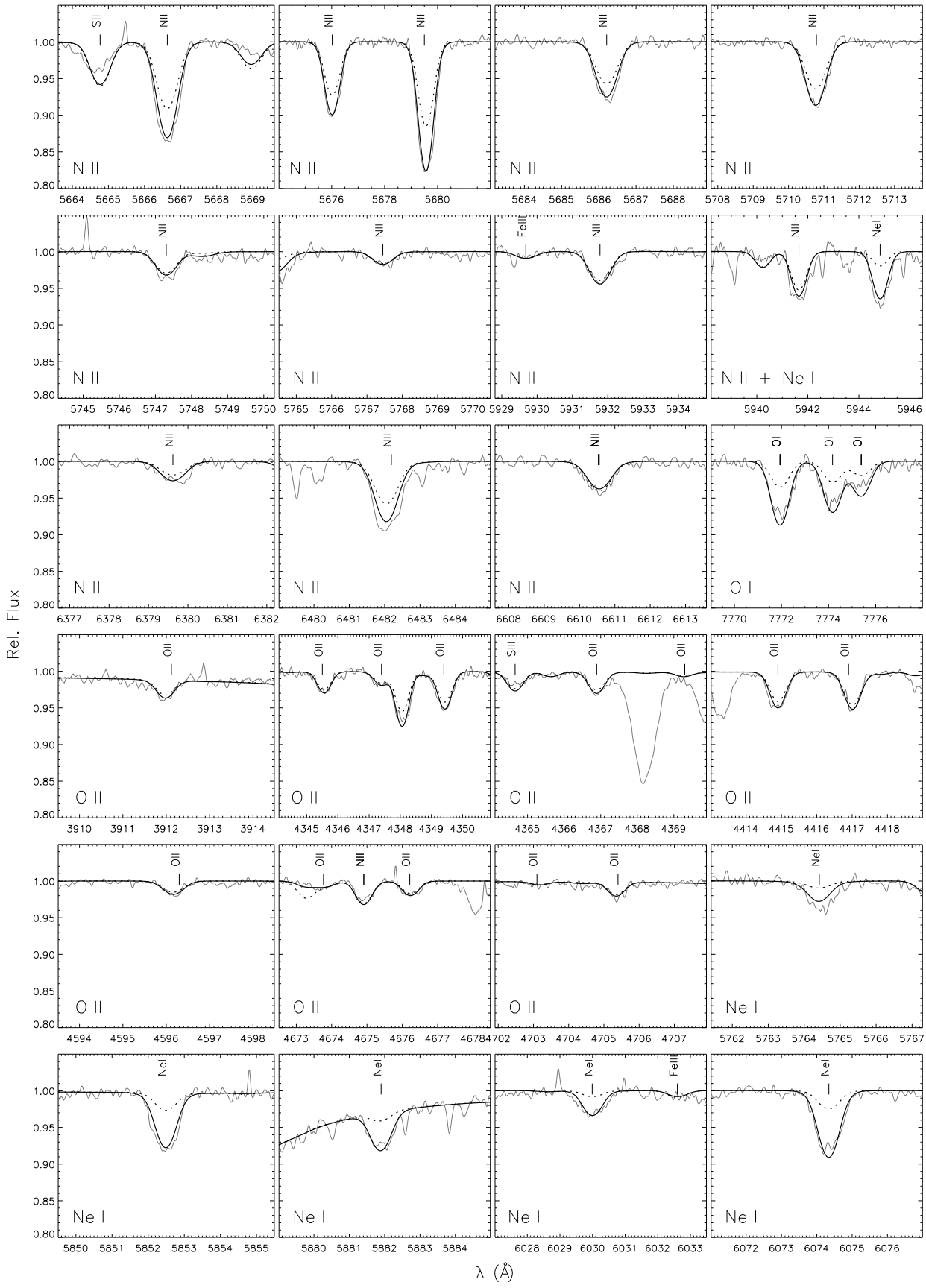

Figure A3. Like Fig. **??**, for analysed N II, O I/II and Ne I lines.

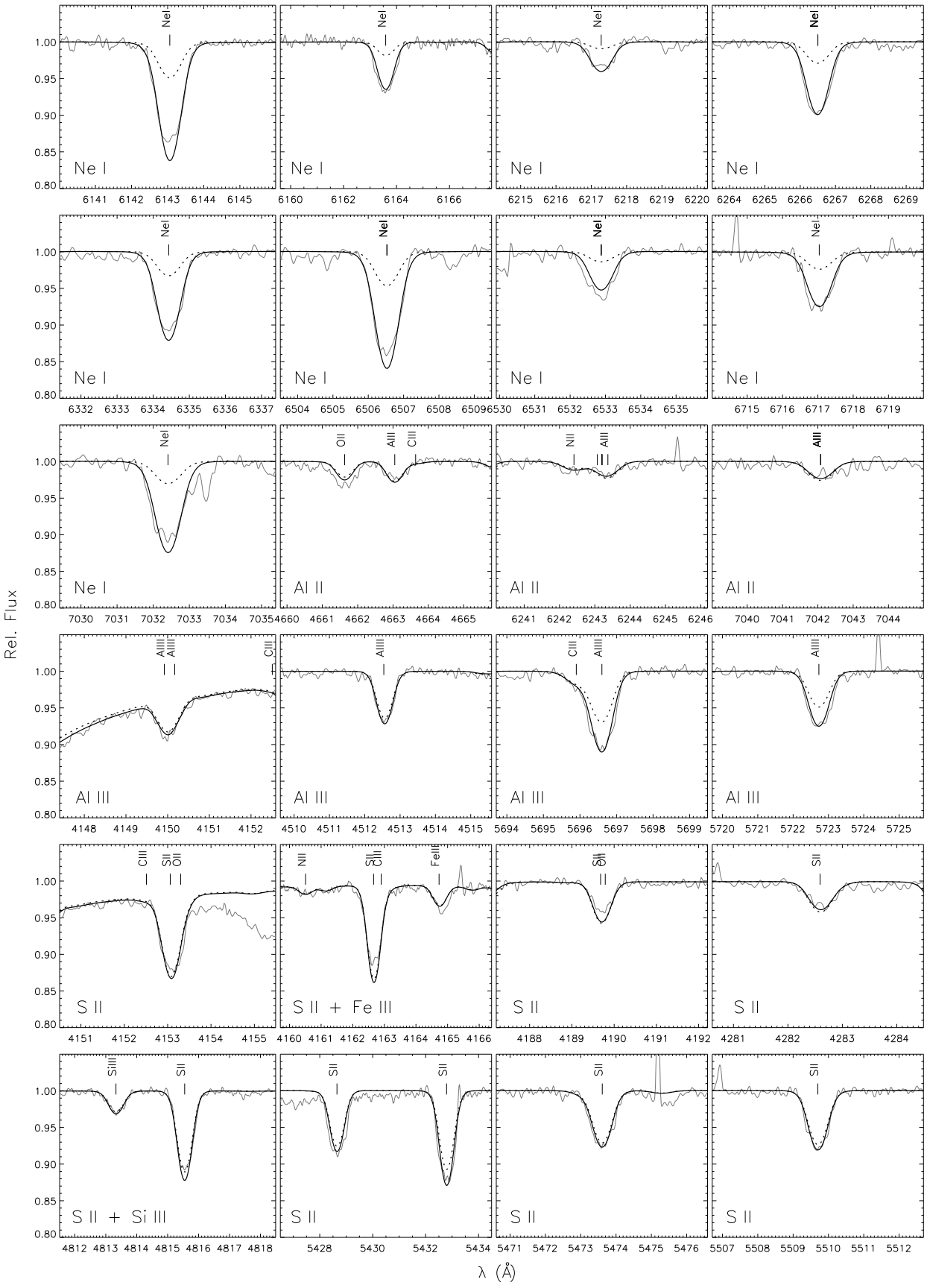

Figure A4. Like Fig. **??**, for analysed Ne I, Al II/III and S II lines.

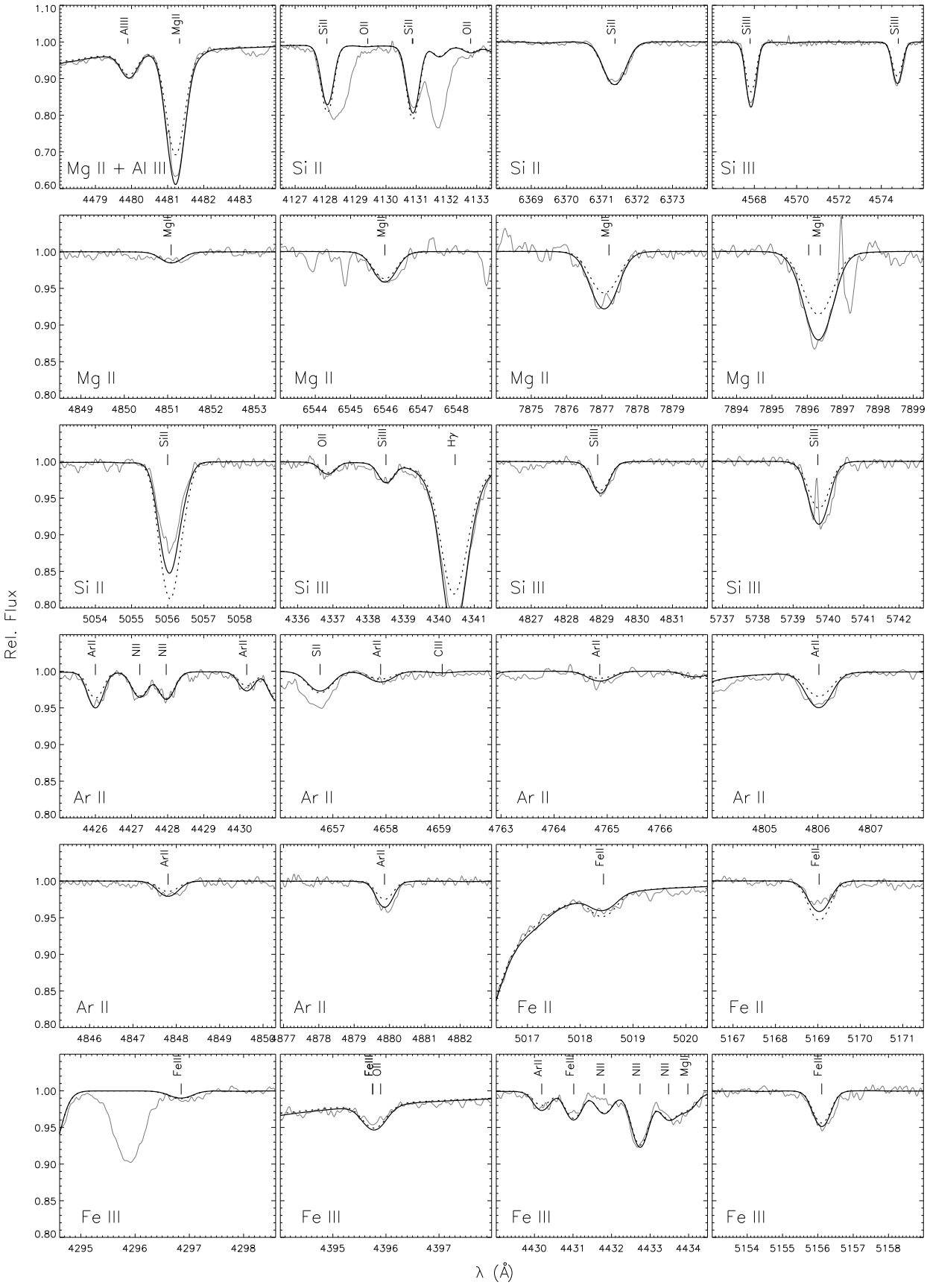

Figure A5. Like Fig. **??**, for analysed Mg II, Si II/III, Ar II and Fe II/III lines.

Table B1. He I line series covered in our spectrum of BD+10°2179

transition	n_{min}	n_{max}	transition	n_{min}	n_{max}
$2s\,^3S - np\,^3P^\circ$	3	4/15*	$3p\,^3P^\circ - ns\,^3S$	7	14
$2s\,^1S - np\,^1P^\circ$	3	15	$3p\,^3P^\circ - nd\,^3D$	7	14
$2p\,^3P^\circ - ns\,^3S$	3	20	$3d\,^3D - np\,^3P^\circ$	7	12
$2p\,^3P^\circ - nd\,^3D$	3	20	$3d\,^3D - nf\,^3F^\circ$	7	14
$2p\,^1P^\circ - ns\,^1S$	3	16	$3d\,^1D - nf\,^1F^\circ$	7	14
$2p\,^1P^\circ - ns\,^1S$	3	16	$3d\,^1D - np\,^1P^\circ$	7	14
$3s\,^3S - np\,^3P^\circ$	5	12	$3p\,^1P^\circ - nd\,^1D$	7	11
$3s\,^1S - np\,^1P^\circ$	6	10	$3p\,^1P^\circ - ns\,^1S$	8	8

* using HST STIS spectra

APPENDIX B: THE HE I SPECTRUM IN BD+10°2179

The peculiar composition of EHe stars in combination with low gravities facilitates a detailed empirical study of the helium line spectrum like in no other class of astronomical objects. While the spectral lines in the optical range can be modelled well with existing line data, see Sect. **??**, this is not the case for neighbouring wavelength ranges to such a degree of completeness. In order to stimulate work to improve, in particular, the availability of line-broadening data, we want to describe the rich He I line features of BD+10°2179 in the optical-UV and the *IzY*-bands covered by our spectra. We therefore also make available the spectrum in electronic form via CDS. Throughout the optical-UV to *IzY* wavelength range coverd by our spectrum we identify dipole-allowed transitions from about 150 multiplets of He I (plus 11 in the HST STIS range). In addition, we want to draw attention to the presence of many forbidden components in the optical spectrum, even several so far unknown ones. The spectral lines were identified based on the compilations of Wiese & Fuhr (2009), Beauchamp & Wesemael (1998), Cann & Thakkar (2002) and the He I line list of Kurucz[1].

B1 Optical-UV

Figure B1 displays the spectrum of BD+10°2179 in the optical-UV range near the atmospheric cut-off to ~3860 Å. This region is dominated by the series limits originating from the $2s\,^1S$, $2p\,^3P^\circ$ and $2p\,^1P^\circ$ levels. The series limit of lines originating from the $2s\,^3S$ level is located farther in the UV, covered by HST STIS spectra. Several lines in this series are strong enough to be identified in a low-resolution spectrum, while the series limit is covered at high resolution. Details on the detected components are summarised in Table B1. Note in particular the very broad transitions to the $^{1,3}D$ terms.

B2 IzY bands

Figure B2 displays the spectrum of BD+10°2179 in the *IzY* bands from ~7000 Å to ~10 200 Å. No efforts have been made to correct for telluric lines – the He I lines in this spectral range are nonetheless identifiable. This spectral range is dominated by the series members originating from the 3*s*, 3*p* and 3*d* levels, see Table B1. The broad features are typically formed by an overlap of several multiplets, facilitated by the close spacing of the involved energy levels.

[1] `http://kurucz.harvard.edu/linelists/gfall/gf0200.all`

Table B2. Known/predicted forbidden He I lines present in BD+10°2179

λ (Å)	transition	λ (Å)	transition
3449	$2s\,^1S - 6d\,^1D$	4025*	$2p\,^3P^\circ - 5f\,^3F^\circ$
3587*	$2p\,^3P^\circ - 9f\,^3F^\circ$	4045	$2p\,^3P^\circ - 5p\,^3P^\circ$
3616	$2s\,^1S - 5d\,^1D$	4142	$2p\,^1P^\circ - 6p\,^1P^\circ$
3634*	$2p\,^3P^\circ - 8f\,^3F^\circ$	4144*	$2p\,^1P^\circ - 6f\,^1F^\circ$
3705*	$2p\,^3P^\circ - 7f\,^3F^\circ$	4383	$2p\,^1P^\circ - 5p\,^1P^\circ$
3711	$2p\,^3P^\circ - 7p\,^3P^\circ$	4387*	$2p\,^1P^\circ - 5f\,^1F^\circ$
3820*	$2p\,^3P^\circ - 6f\,^3F^\circ$	4470	$2p\,^3P^\circ - 4f\,^3F^\circ$
3830	$2p\,^3P^\circ - 6p\,^3P^\circ$	4517	$2p\,^3P^\circ - 4p\,^3P^\circ$
3971	$2s\,^1S - 4f\,^1F^\circ$	4911	$2p\,^1P^\circ - 4p\,^1P^\circ$
3972	$2s\,^1S - 4d\,^1D$	4921	$2p\,^1P^\circ - 4f\,^1F^\circ$
4008	$2p\,^1P^\circ - 7p\,^1P^\circ$	5042	$2s\,^1S - 3d\,^1D$
4009*	$2p\,^1P^\circ - 7f\,^1F^\circ$		

* presence inferred because of line asymmetries

B3 Forbidden components in the optical

Extreme helium stars are a testbed for the detection of isolated forbidden components of He I transitions. Harrison & Jeffery (1997) detected all ten forbidden components listed by Underhill (1966) in their spectrum of the EHe star HD 144941 in the wavelength range 3840–4960 Å[2]. We extend this list to 23 known/predicted lines covered by the wavelength range of our spectra. To our knowledge, these additional forbidden components (electronic quadrupole transitions) are observationally confirmed for the first time by the present work, summarised in Table B2 and visualised in Figure B3. Note the good agreement with the asymmetric line shapes predicted by Beauchamp & Wesemael (1998). The presence of several forbidden components as marked in Table B2 is inferred because of line asymmetries. Line separations between the allowed and forbidden components amount in these cases from a maximum of 0.64 Å for [He I] λ4025 Å to a minimum value of 0.17 Å for [He I] λ3705 Å. We cannot confirm the presence of the forbidden component $\lambda\lambda$ 6632 Å (the region is affected by an artifact from the data reduction). Additional (weak) transitions at $\lambda\lambda$ 3809, 3165, 4054 and 6068 Å and forbidden components in the HST STIS range at $\lambda\lambda$ 2935 and 2823 Å with lower levels of $n = 2$ are also not detected, as well as the forbidden components from lower levels with $n = 3$ like $\lambda\lambda$ 8315, 9360, 9616 Å. Reasons for these are manifold: the transitions being too weak to be detected, blends, insufficient S/N, insufficient resolution of the low-resolution HST STIS data, uncorrectable contamination with nearly opaque telluric lines.

The inspection of the optical-UV spectrum with overlaid identifiers of the known He I lines shows a conspicuous series of isolated or blended features between the lines of the higher $2p\,^3P^\circ$ to $nd\,^3D$ and $ns\,^3S$ series, see the 4th and 5th panels of Fig. B1. This so far undocumented series is produced by E2 transitions from $2p\,^3P^\circ$ to $np\,^3P^\circ$ with $n \geq 8$, i.e. transitions to higher levels than described in any previous work. We characterise this series in Table B3, providing information on the transition, wavelengths in air λ_{air} and vacuum λ_{vac}, level energies, statistical weights and transition type. The data are given from $n = 7$ to 20, despite we can infer the presence of this component only up to $n = 16$ or 17 because of line asymmetries. Higher series members may be detectable in EHe stars with lower gravities than BD+10°2179.

[2] However, resolving the λ3972 Å component (and λ3971 Å) was hampered by the relatively strong Hε line in HD 144931, nearly absent here because of the lower hydrogen content of BD+10°2179.

Table B3. New detections and extension of the $2p\,^3\mathrm{P}^\circ - np\,^3\mathrm{P}^\circ$ forbidden line spectrum of He I

Transition	λ_{air} (Å)	λ_{vac} (Å)	E_i–E_k (cm^{-1})	g_i–g_k	Type
$2p\,^3\mathrm{P}^\circ - 7p\,^3\mathrm{P}^\circ$	3710.85	3711.90	169086.9085 – 196027.316	9–9	E2
$2p\,^3\mathrm{P}^\circ - 8p\,^3\mathrm{P}^\circ$	3638.00	3639.04	169086.9085 – 196566.712	9–9	E2
$2p\,^3\mathrm{P}^\circ - 9p\,^3\mathrm{P}^\circ$	3589.85	3590.87	169086.9085 – 196935.331	9–9	E2
$2p\,^3\mathrm{P}^\circ - 10p\,^3\mathrm{P}^\circ$	3556.26	3557.27	169086.9085 – 197198.332	9–9	E2
$2p\,^3\mathrm{P}^\circ - 11p\,^3\mathrm{P}^\circ$	3531.83	3532.84	169086.9085 – 197392.720	9–9	E2
$2p\,^3\mathrm{P}^\circ - 12p\,^3\mathrm{P}^\circ$	3513.53	3514.53	169086.9085 – 197540.190	9–9	E2
$2p\,^3\mathrm{P}^\circ - 13p\,^3\mathrm{P}^\circ$	3499.43	3500.43	169086.9085 – 197654.830	9–9	E2
$2p\,^3\mathrm{P}^\circ - 14p\,^3\mathrm{P}^\circ$	3488.34	3489.34	169086.9085 – 197745.650	9–9	E2
$2p\,^3\mathrm{P}^\circ - 15p\,^3\mathrm{P}^\circ$	3479.45	3480.45	169086.9085 – 197818.830	9–9	E2
$2p\,^3\mathrm{P}^\circ - 16p\,^3\mathrm{P}^\circ$	3472.22	3473.21	169086.9085 – 197878.690	9–9	E2
$2p\,^3\mathrm{P}^\circ - 17p\,^3\mathrm{P}^\circ$	3466.25	3467.24	169086.9085 – 197928.260	9–9	E2
$2p\,^3\mathrm{P}^\circ - 18p\,^3\mathrm{P}^\circ$	3461.27	3462.26	169086.9085 – 197969.750	9–9	E2
$2p\,^3\mathrm{P}^\circ - 19p\,^3\mathrm{P}^\circ$	3457.07	3458.06	169086.9085 – 198004.850	9–9	E2
$2p\,^3\mathrm{P}^\circ - 20p\,^3\mathrm{P}^\circ$	3453.49	3454.48	169086.9085 – 198034.800	9–9	E2

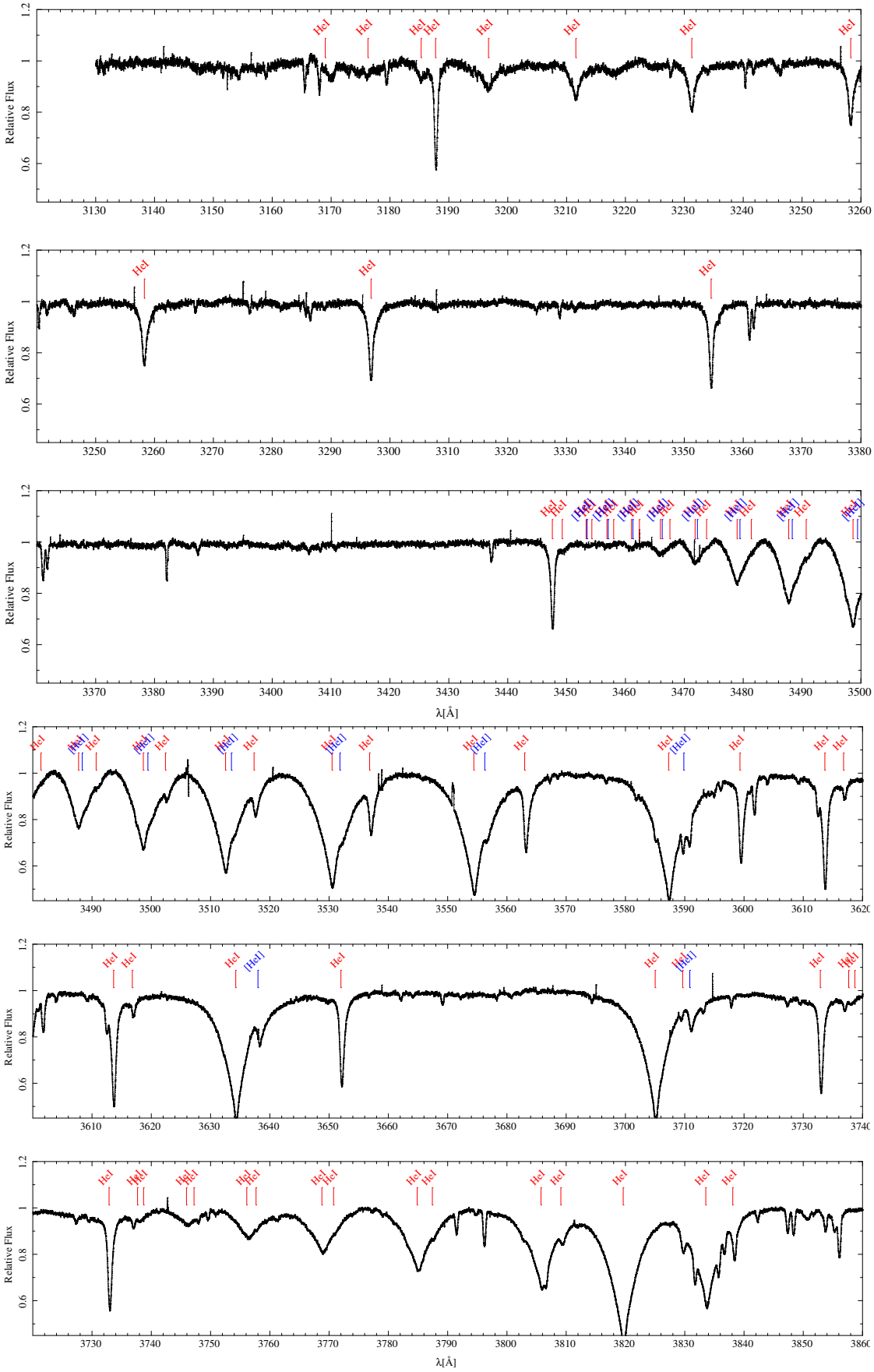

Figure B1. He I lines in the optical-UV as traced by our UVES spectrum. Blue marked are the new detected series of forbidden He I given in Table B3.

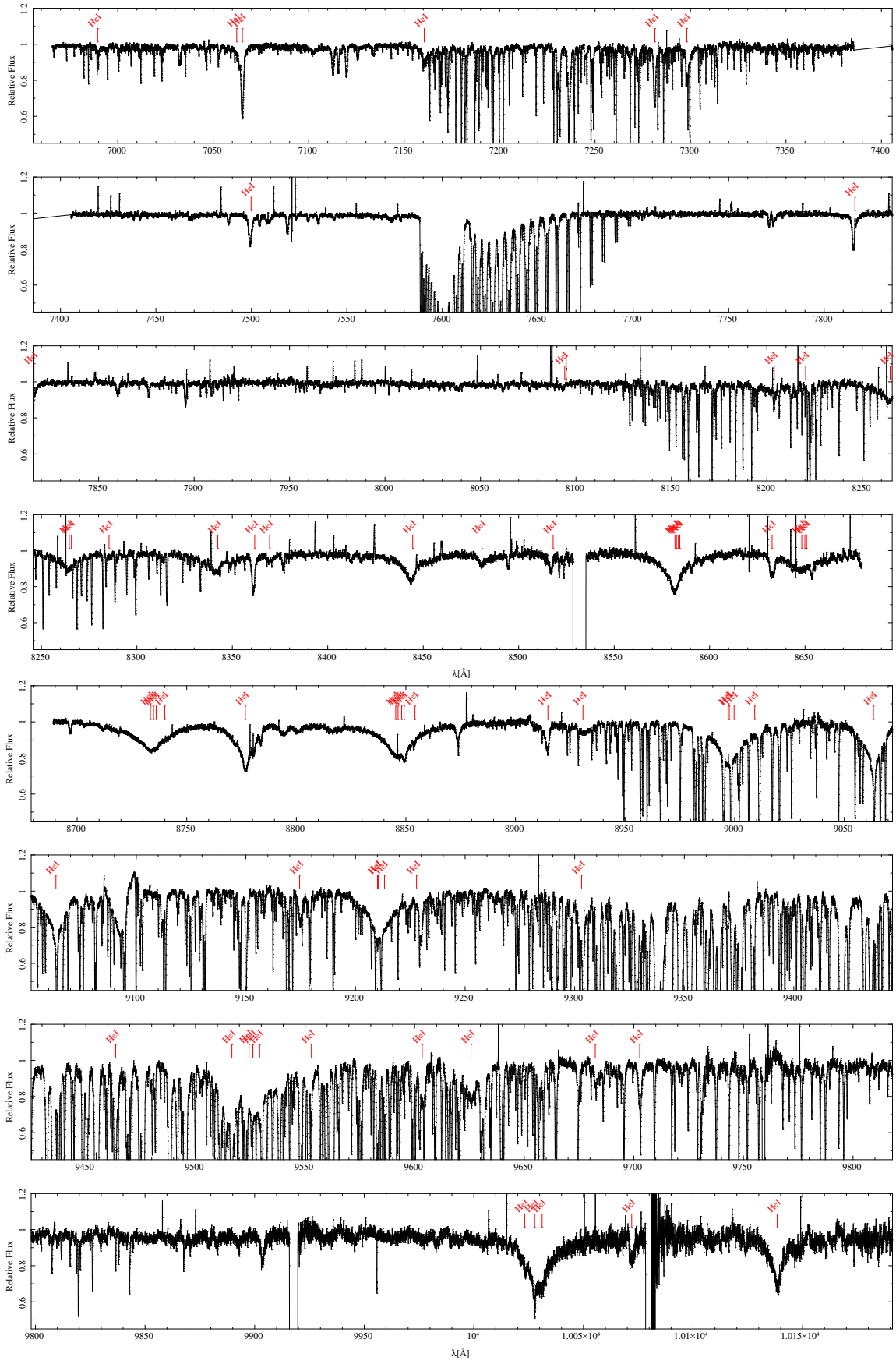

Figure B2. He I lines in the near-IR *IzY* bands as traced by our UVES and FEROS spectra.

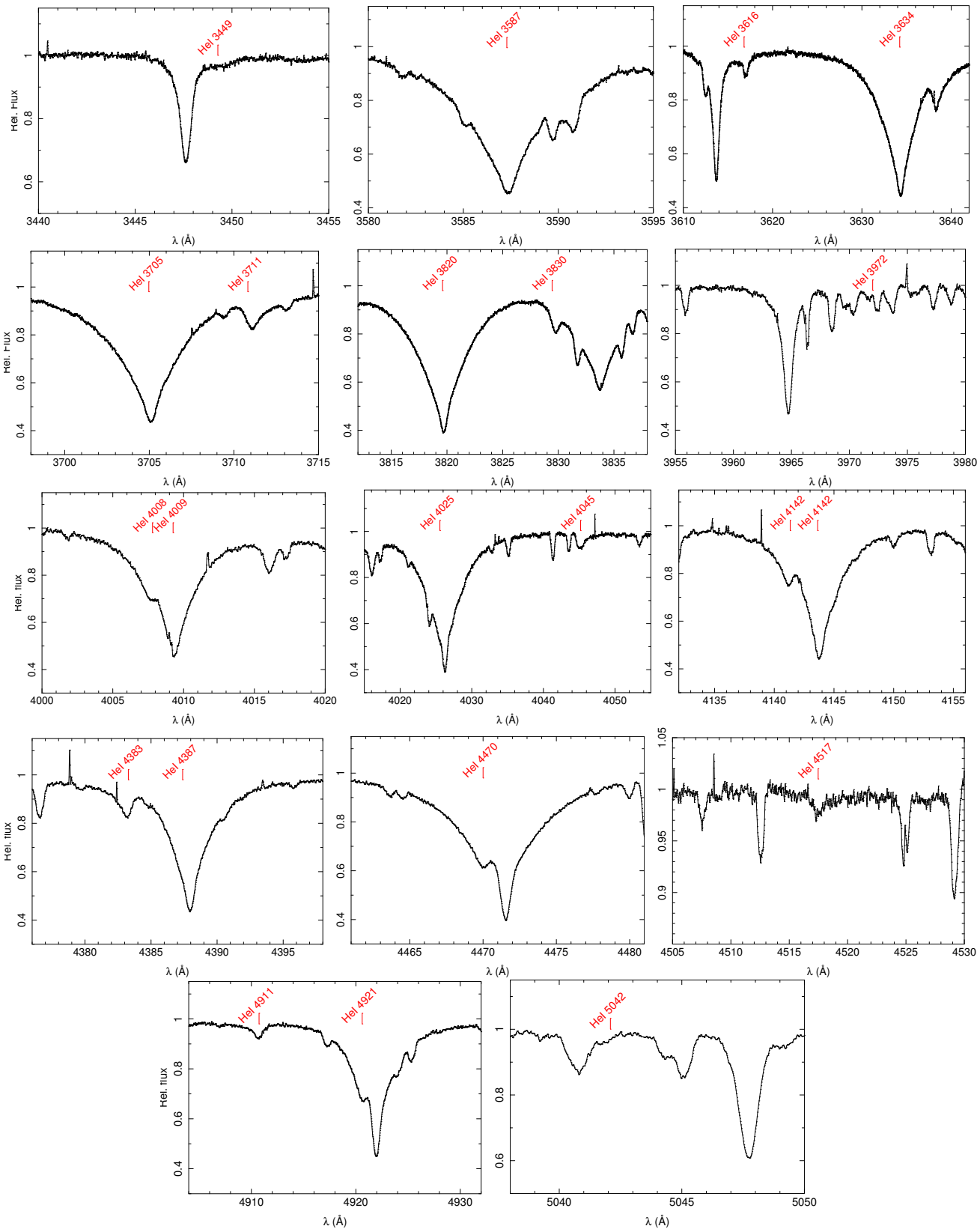

Figure B3. Isolated forbidden He I components in the optical spectrum.

REFERENCES

Bates D. R., Damgaard A., 1949, Phil. Trans. R. Soc. London, Ser. A,, 242, 101

Beauchamp A., Wesemael F., 1998, ApJ, 496, 395

Becker S. R., Butler K., 1989, A&A, 209, 244

Callegari F., Trigueiros A. G., 1998, ApJS, 119, 181

Cann N. M., Thakkar A. J., 2002, J. Phys. B: At. Mol. Opt. Phys., 35, 421

Cowley C. R., 1971, The Observatory, 91, 139

Froese Fischer C., Tachiev G., 2004, At. Data Nucl. Data Tables, 87, 1

Froese Fischer C., Tachiev G., Irimia A., 2006, At. Data Nucl. Data Tables, 92, 607

Fuhr J. R., Wiese W. L., 1998, in CRC Handbook of Chemistry and Physics, 79th edn., ed. D. R. Lide (Boca Raton: CRC Press)

Fuhr J. R., Martin G. A., Wiese W. L., 1988, J. Phys. & Chem. Ref. Data., 17

Griem H. R., 1964, Plasma spectroscopy (New York: Mc-Graw-Hill)

Griem H. R., 1974, Spectral line broadening by plasmas (New York: Academic Press)

Harrison P. M., Jeffery C. S., 1997, A&A, 323, 177

Kurucz R., Bell B., 1995, Kurucz CD-ROM No. 23. Cambridge, Mass.: SAO,

Lanz T., Dimitrijevic M. S., Artru M.-C., 1988, A&A, 192, 249

Luo D., Pradhan A. K., 1989, J. Phys. B: At. Mol. Opt. Phys., 22, 3377

Mar S., Pérez C., González V. R., Gigosos M. A., del Val J. A., de la Rosa I., Aparicio J. A., 2000, A&AS, 144, 509

Morel T., Butler K., 2008, A&A, 487, 307

Nahar S. N., 2002, At. Data Nucl. Data Tables, 80, 205

Underhill A. B., ed. 1966, The early type stars (Dordrecht: Reidel)

Vidal C. R., Cooper J., Smith E. W., 1973, ApJS, 25, 37

Wiese W. L., Fuhr J. R., 2009, J. Phys. & Chem. Ref. Data., 38, 565

Wiese W. L., Smith M. W., Miles B. M., 1969, Nat. Stand. Ref. Data Ser., Nat. Bur. Stand. (US), NSRDS-NBS 22, Vol. 2

Wiese W. L., Fuhr J. R., Deters T. M., 1996, J. Phys. & Chem. Ref. Data., Monograph 7